High-Resolution Oscillating Steady-State fMRI using Patch-Tensor Low-Rank Reconstruction

Supplementary Material

Shouchang Guo, Jeffrey A. Fessler, and Douglas C. Noll

This supplemental material presents: (1) OSSI signal properties including example OSSI images and time courses before and after Fourier transform, and tensor low-rankness for patch-tensors at different regions of the brain; (2) the incoherent trajectory rotation schemes for both retrospective and prospective undersampling; (3) reconstruction details including effects of overlapping time blocks and regularization parameter selection based on impulse perturbation; (4) reconstruction comparisons for 2D retrospective and prospective undersampling; (5) other reconstruction methods including 4D patch-tensor low-rank and multi-scale tensor low-rank; (6) reconstruction results of a different subject.

I. OSSI Signal Properties

This section presents in-vivo OSSI images and time courses, and demonstrates local low-rankness of OSSI fMRI time-series. Figure S1 shows 2 cycles of OSSI fast time images with periodic oscillation patterns. Figure S2 provides example time courses from non-activated and activated ROIs of the OSSI images. Figure S3 gives 1D Fourier transformed (along fast time) results for the complex time series corresponding to the images in Figure S1, and Figure S4 presents the Fourier transformed time courses of Figure S2. OSSI images are not very sparse before or after Fourier transform due to the nonlinear oscillations. Figure S5 gives log-scale singular value plots of non-activated and activated 3D patch-tensors from an OSSI fMRI time block.

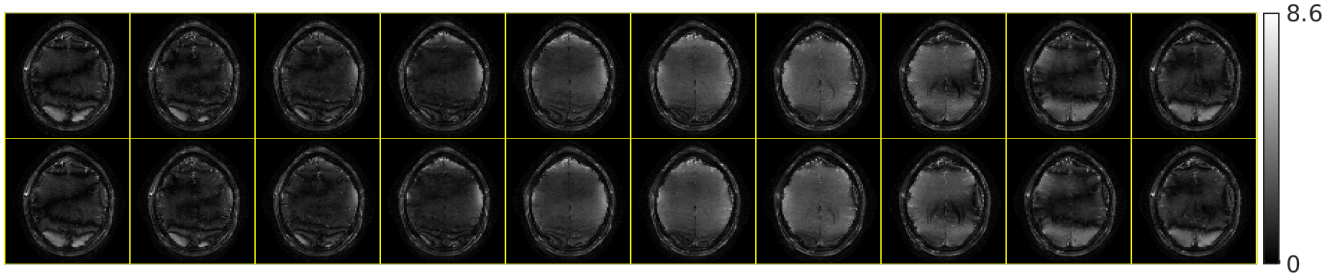

Fig. S1. Example OSSI fast time magnitude images for 2 cycles of the periodic oscillations.

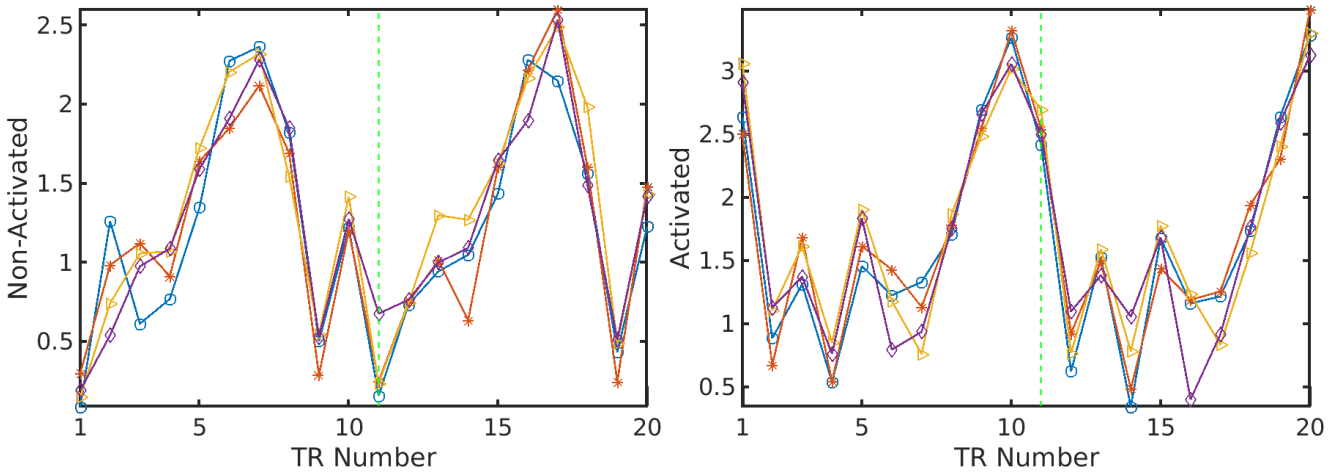

Fig. S2. OSSI fast-time time courses (magnitudes) of 4 different voxels within a brain region that is not activated (left) or activated (right). The signal oscillation pattern repeats every n_c = 10 TRs, as indicated by the vertical green dashed line.

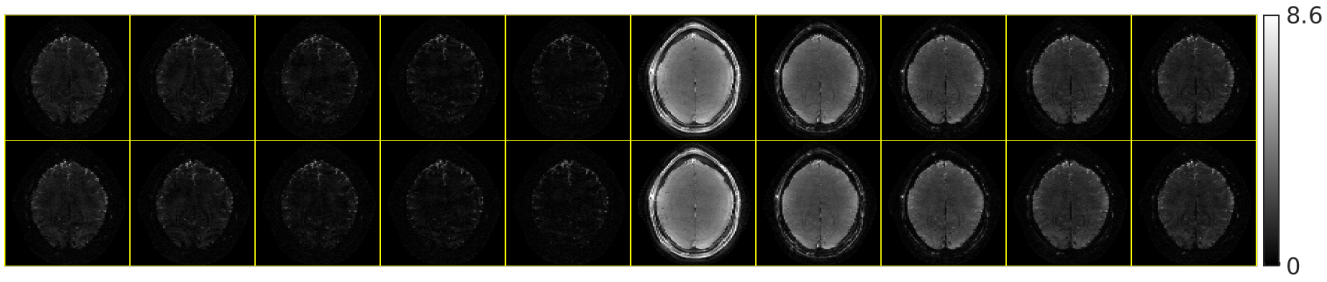

Fig. S3. Results after taking 1D Fourier transform along fast time of the OSSI images shown in Figure S1. Magnitude is shown and temporal frequency 0 is in "middle" (6th image from left). OSSI fast time images are not very sparse in the Fourier domain.

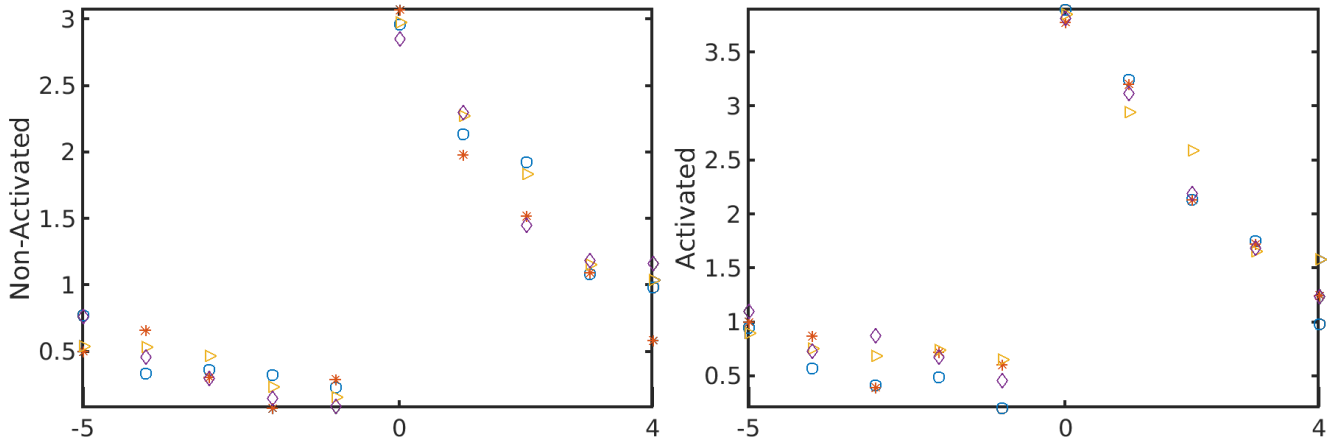

Fig. S4. Results after taking 1D Fourier transform along fast time (every n_c = 10 TRs) of the OSSI time courses in Figure S2. Magnitude of one cycle is shown and temporal frequency 0 is in "middle". OSSI fast time signals are not very sparse in the Fourier domain.

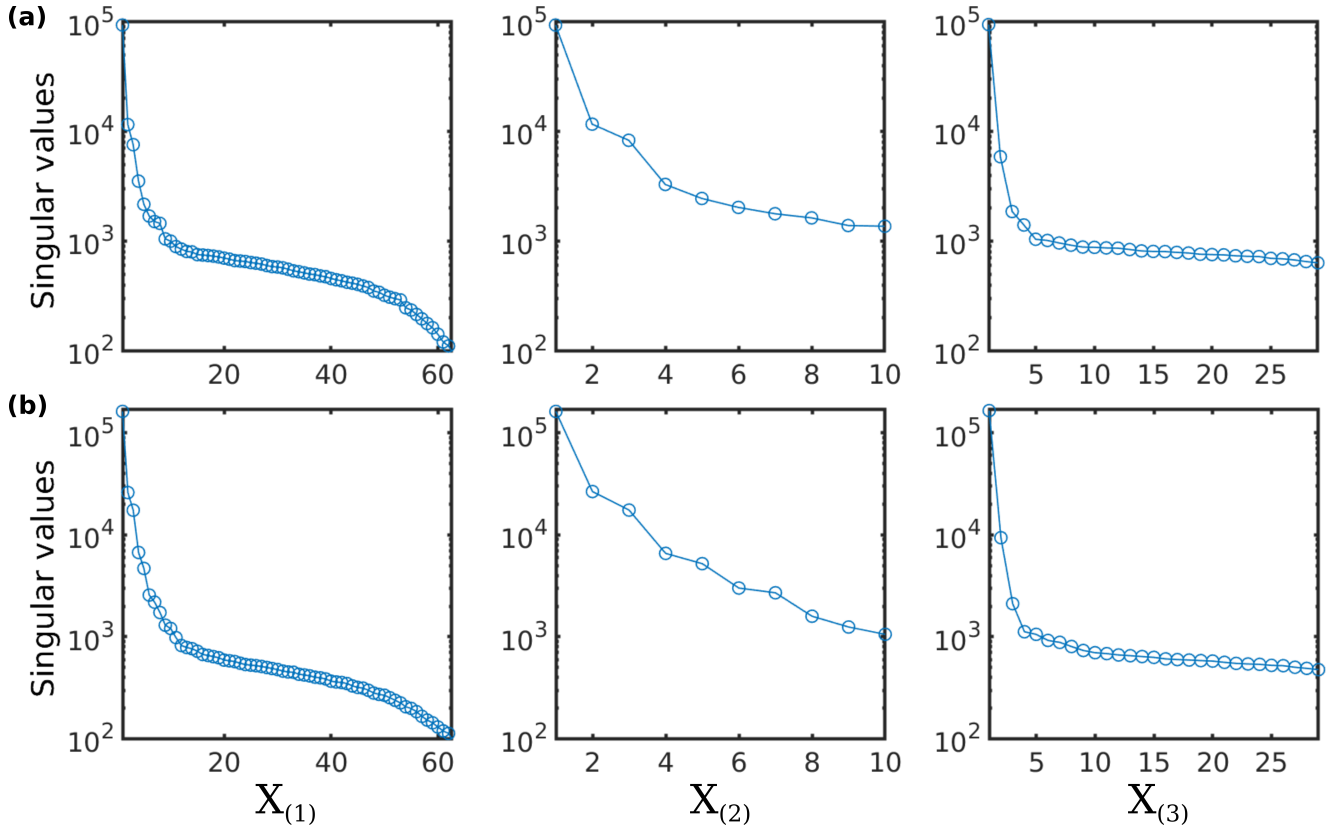

Fig. S5. Log-scale singular value plots for all 3 unfoldings of a 3D patch-tensor (a) at the center of the brain with no activation (b) at the activation region. For both activated and non-activated patch-tensors, the unfoldings show a similar pattern that $\boldsymbol{X}_{(3)}$ has lower rank than $\boldsymbol{X}_{(1)}$ and $\boldsymbol{X}_{(2)}$.

II. Incoherent Sampling Pattern

This section illustrates how the proposed spiral rotations help increase temporal incoherence for OSSI acquisition. For prospective undersampling, the baseline rotation of $ga \cdot k$ for frame k leads to an angle difference of $10ga \bmod 360° = 32°$ between consecutive slow time points. With the additional angle of $ga \cdot \lfloor k/n_c \rfloor$, the angle difference becomes $11ga \bmod 360° = 144°$, which increases sampling incoherence along slow time as compared in Figure S6. Similarly for retrospective undersampling, the angle difference between undersampled slow time points changes from $90ga \bmod 360° = -68°$ to $92ga \bmod 360° = 155°$ with improved incoherence as in Figure S7.

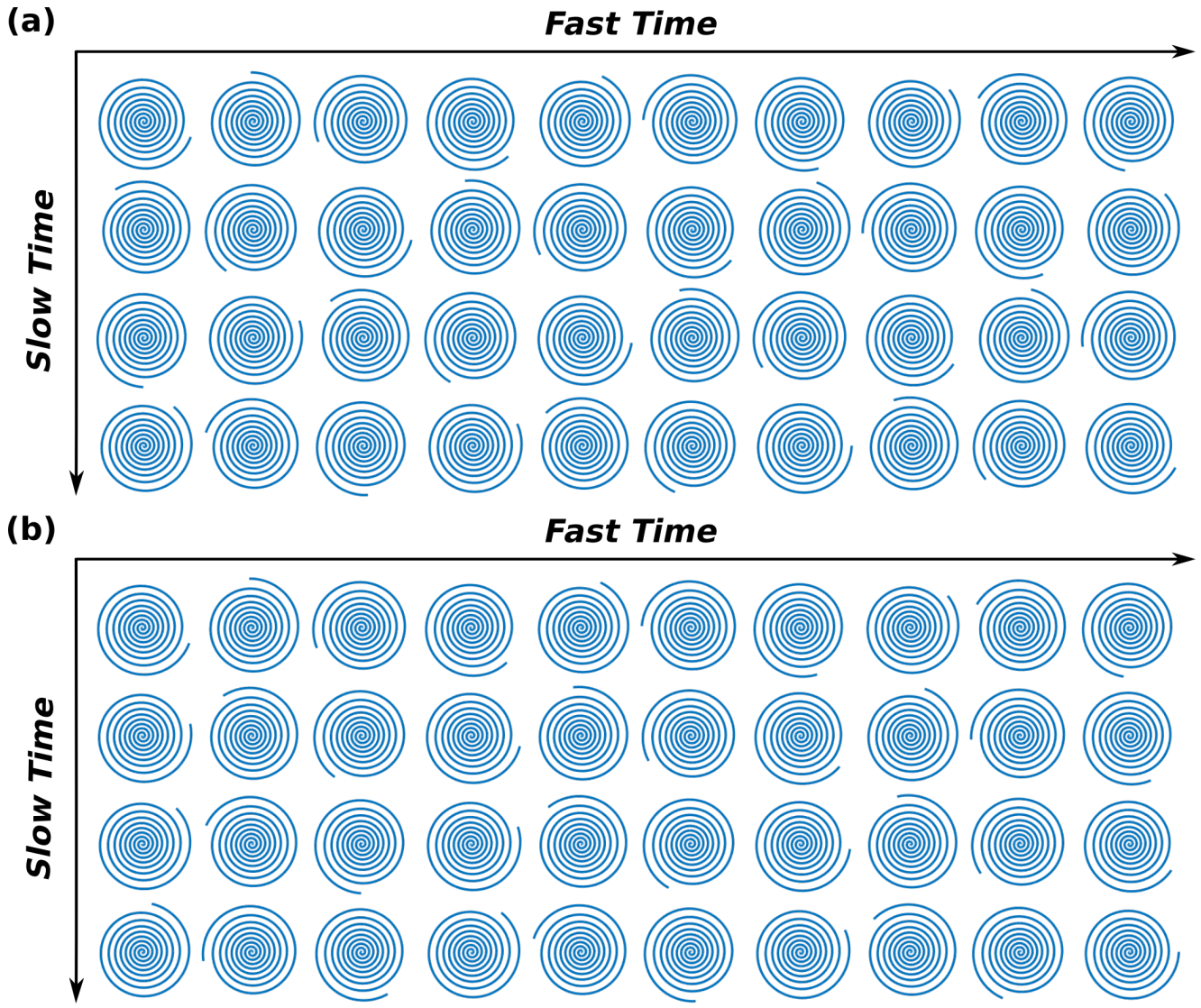

Fig. S6. Demonstration of the incoherent rotations for 2D prospective undersampling. The proposed scheme of $\boldsymbol{ga \cdot k + ga \cdot \lfloor k/n_c \rfloor}$ in (a) increases the sampling incoherence along slow time compared to a baseline rotation scheme of $\boldsymbol{ga \cdot k}$ in (b).

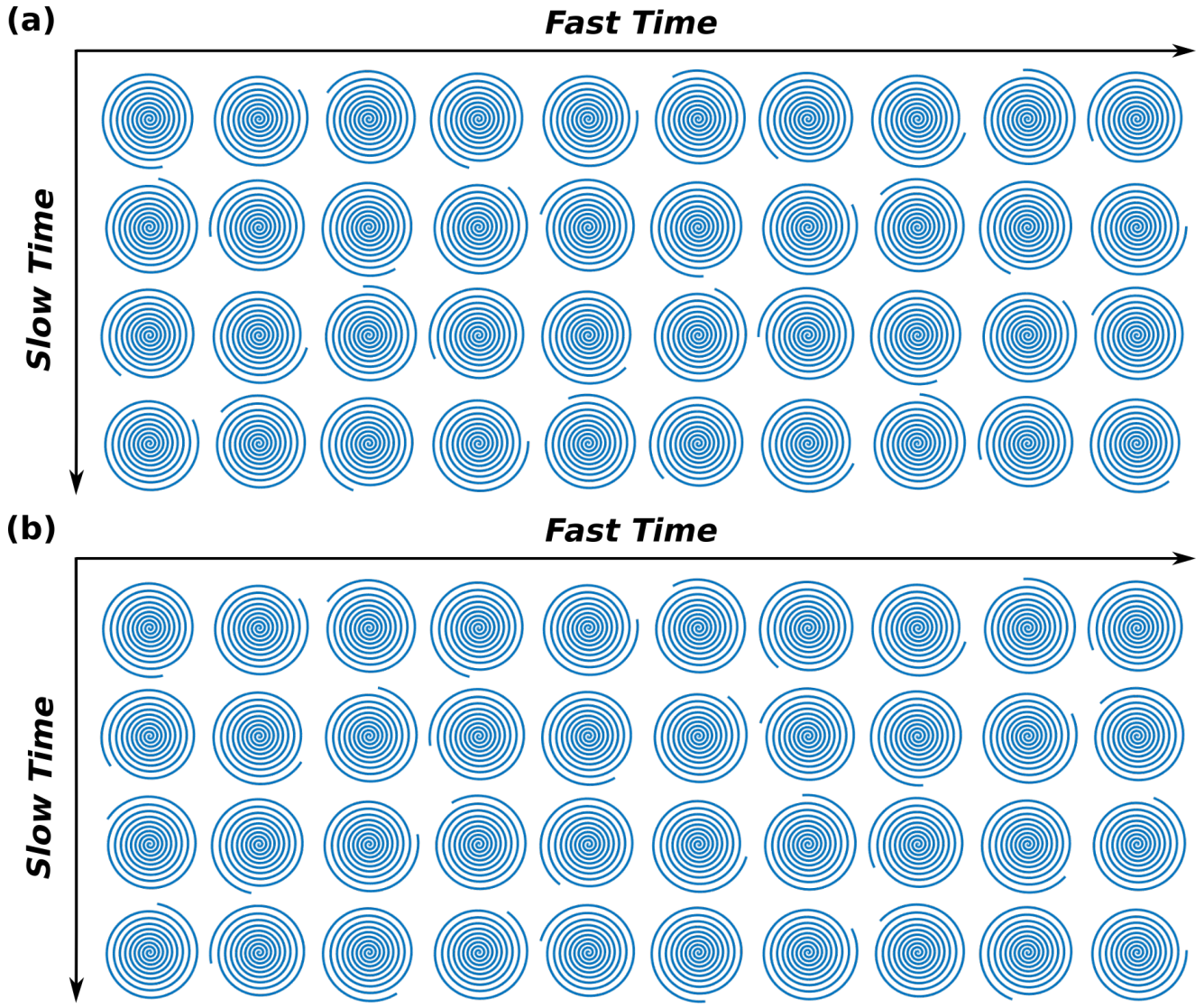

Fig. S7. Demonstration of the incoherent rotations for 2D retrospective undersampling. The proposed scheme of $ga \cdot k + 2 \cdot ga \cdot \lfloor k/n_c/n_i \rfloor$ in (a) increases the sampling incoherence along slow time compared to a baseline rotation scheme of $ga \cdot k$ in (b).

III. Reconstruction Adjustment

This section presents practical adjustments to the reconstruction methods including local impulse responses for regularization parameter selection and structuring overlapping time blocks for the OSSI fMRI time course.

A. Regularization Parameter Selection

The local impulse response profiles in Figure S8 demonstrate that we have tuned the different reconstruction methods so that they are regularizing the data by similar amounts without excessive spatial or temporal smoothing.

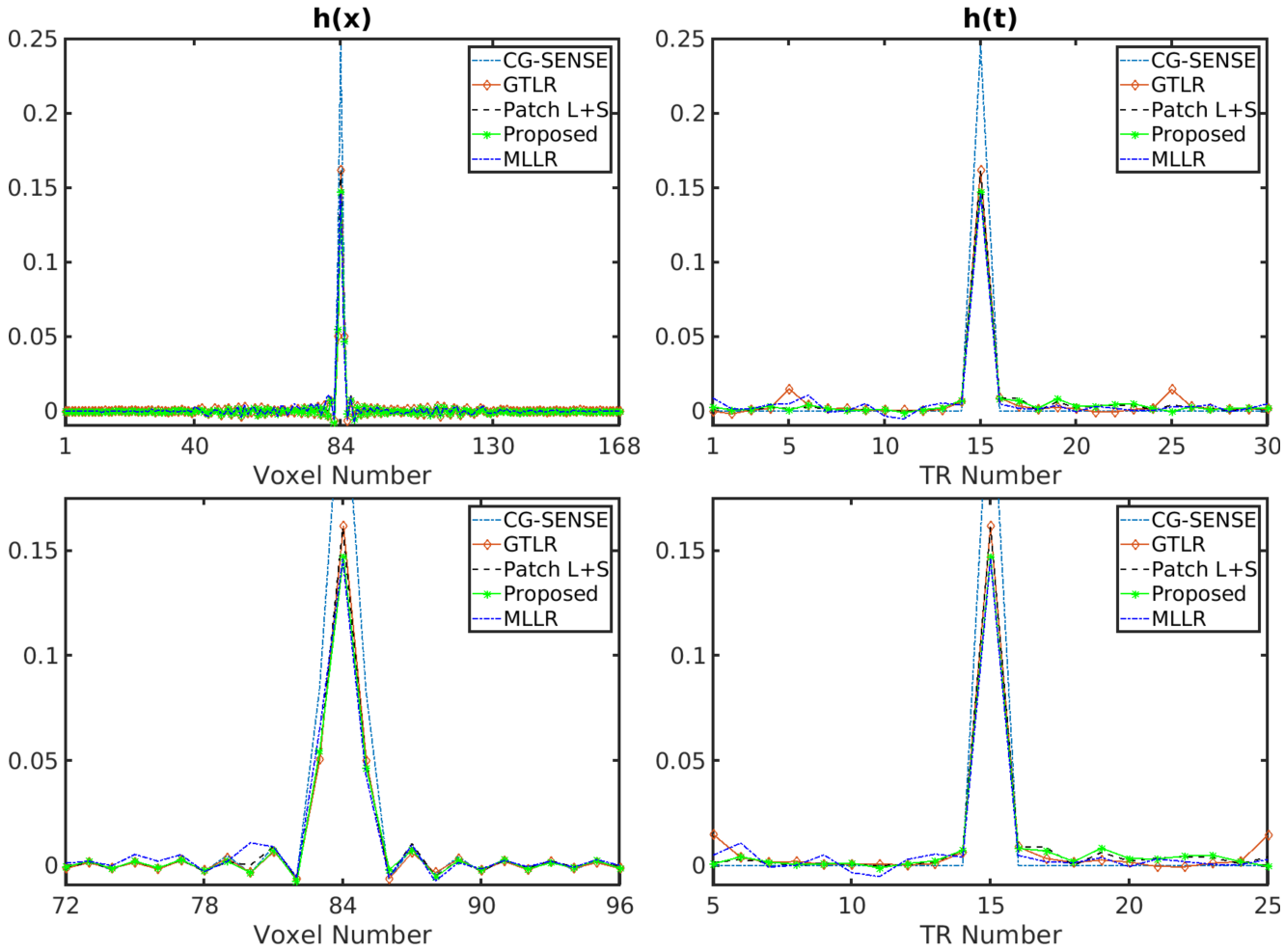

Fig. S8. Impulse responses of different reconstructions along spatial dimension (left) and temporal dimension (right). Enlarging the central part of the impulse responses (bottom left and right) shows that impulse responses for different reconstruction models are of similar magnitudes and preserve spatial and temporal resolution with relatively small tails. Because the perturbation of $\delta(j,t)$ added to the image domain is real, and the imaginary parts of the impulse responses are small enough to be neglected, the real parts of the impulse responses are shown.

B. Overlapping Time Blocks

Figure S9 illustrates ranges of overlapping time blocks and the formation of the entire reconstructed time course after discarding the overlapping portions. Figure S10 compares activated time courses and spectra from reconstructions using non-overlapping time blocks or overlapping time blocks. With carefully adjusted regularization parameters, reconstructing overlapping blocks or non-overlapping blocks led to similar results.

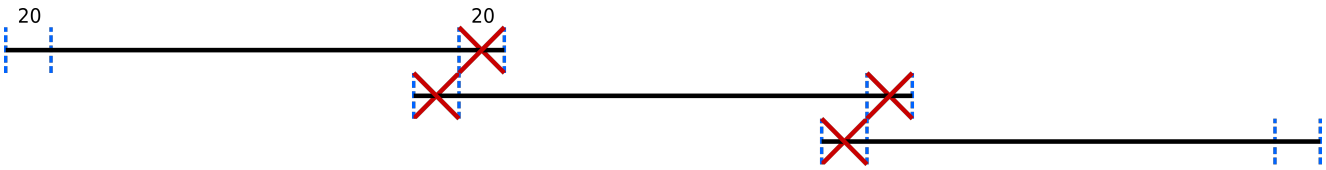

Fig. S9. The OSSI fMRI time course is broken into overlapping time blocks of about 300 time points (denoted by black horizontal lines) for reconstruction. The overlapping portion of 20 time points at both ends of the time blocks (denoted by red crosses) are discarded after reconstruction except for the beginning and ending portions of the whole time series.

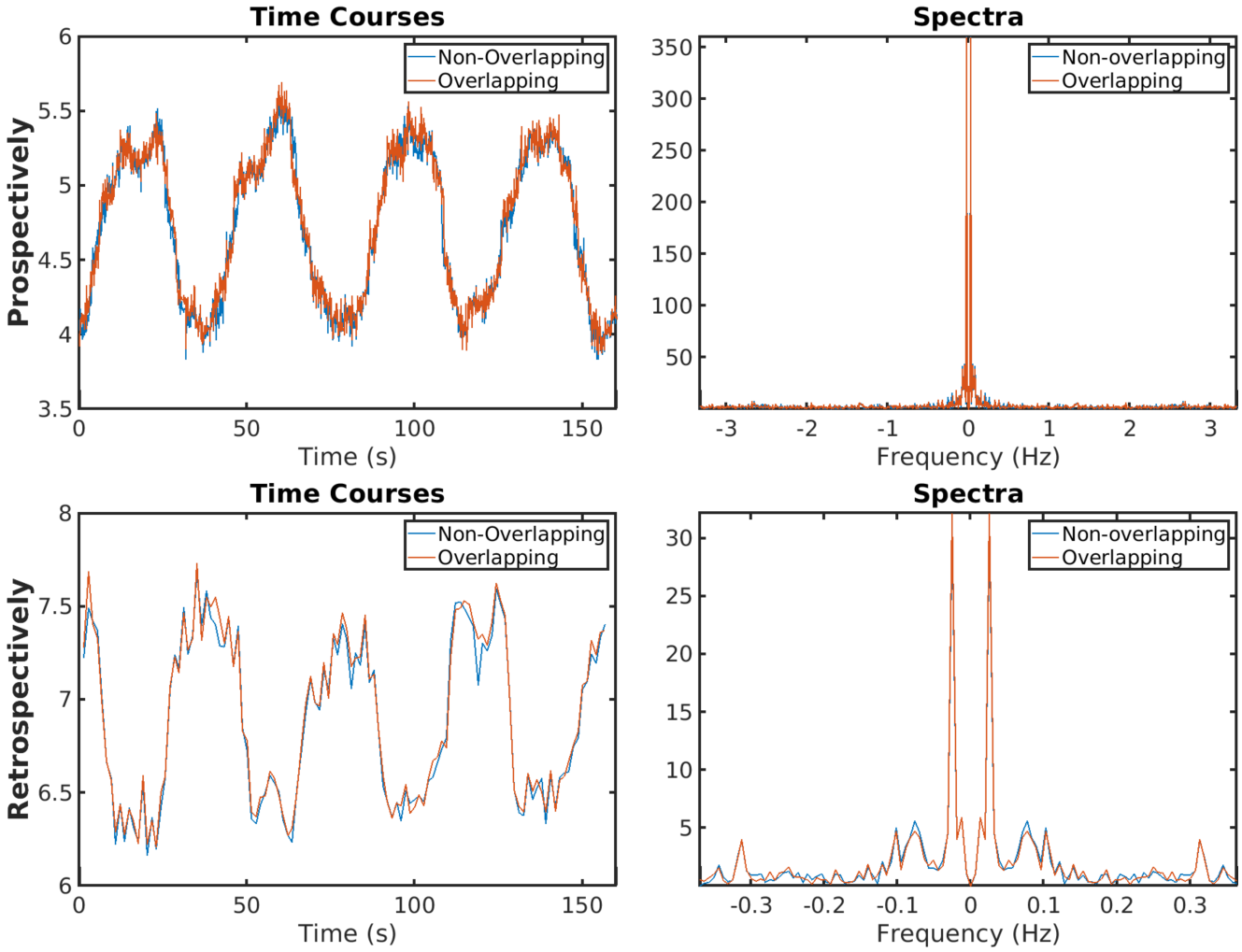

Fig. S10. For both prospectively and retrospectively undersampled data, reconstructing overlapping time blocks or non-overlapping time of the whole OSSI fMRI time course leads to very similar time courses and spectra.

IV. Comparison and Results

This section presents additional reconstruction results for 2D retrospectively and prospectively undersampled data.

A. 2D Retrospectively Undersampling

Figure S11 shows difference maps of 2-norm combined reconstructions compared to the mostly sampled case. ROC curves for the activation maps of different reconstruction approaches in Figure S12 shows that the proposed approach leads to the largest area under the ROC curve (AUC). Mostly sampled activation at the lower third of the brain was used as ground truth, and the activation threshold ranges from -0.1 to 0.99 with a 0.001 spacing. Figure S13 presents autocorrelations of the correlation maps for different reconstructions. It verifies that the proposed approach preserves spatial resolution for fMRI. Figure S14 shows the low-rank and sparse components (10 fast time points) of the patch-tensor low-rank plus sparse reconstruction. The sparse component is small and contains little information.

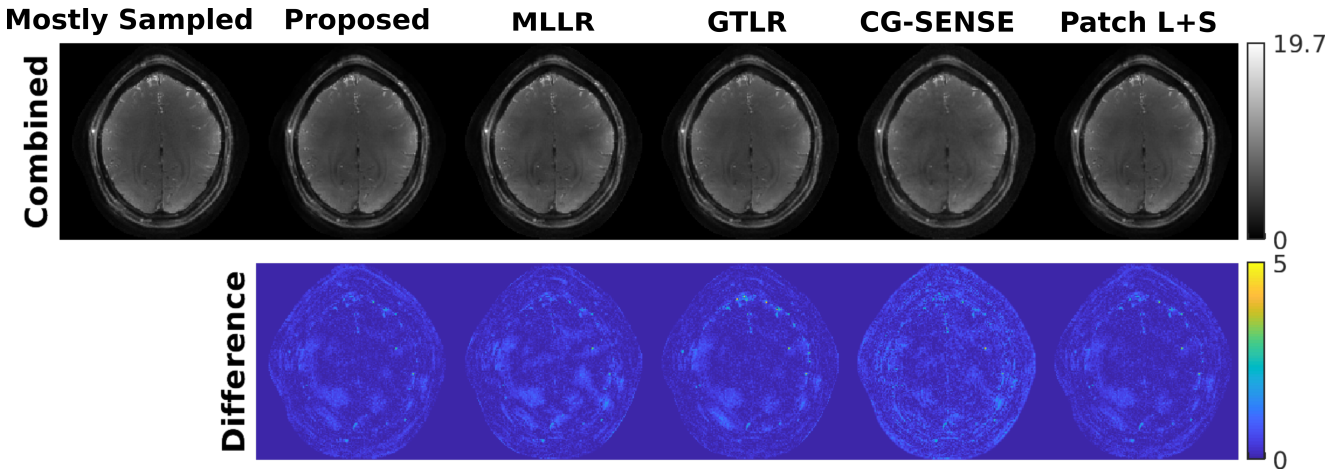

Fig. S11. Reconstructed images and difference maps (compared to the mostly sampled reconstruction) of different models after 2-norm combination. The proposed approach presents less residual in the difference map.

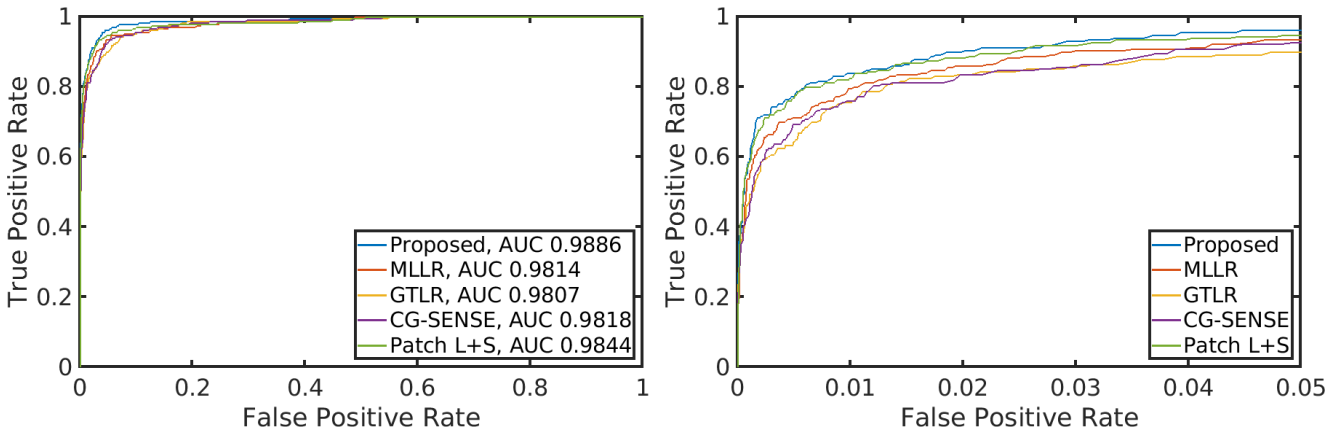

Fig. S12. ROC curves of different reconstruction approaches with mostly sampled activation at the lower third of the brain as ground truth. The proposed method outperforms other approaches with the largest area under the ROC curve (left). The ROC curve of the proposed approach is also the closest to the top left corner, especially for the reasonable range with false positive rate less than 0.05 (right).

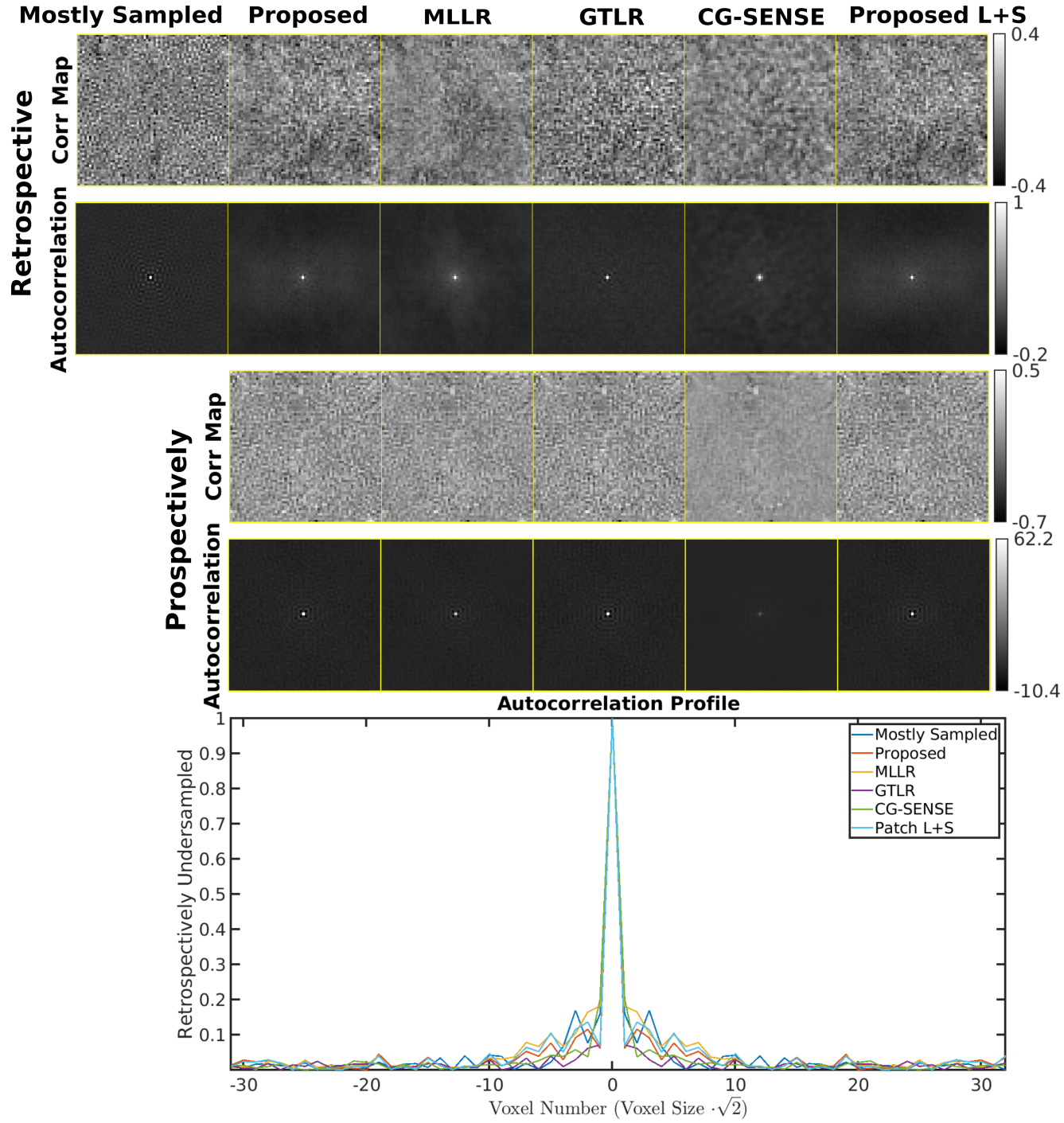

Fig. S13. Correlation maps and normalized autocorrelations of the correlation map for the different reconstructions at the center of the brain without activation. The proposed model results in similar autocorrelation profiles along diagonal as the mostly sampled reconstruction.

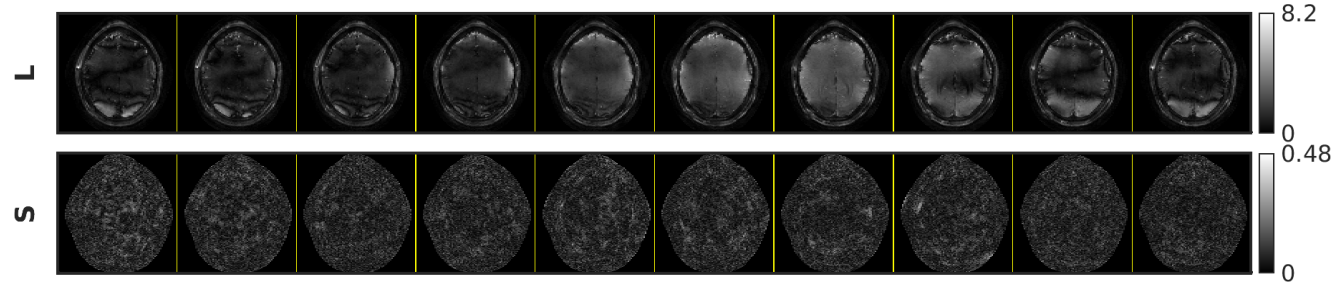

Fig. S14. The low-rank and sparse components (first 10 fast time points) of the patch-tensor low-rank plus sparse reconstruction with 2D retrospectively undersampled data. The sparse component is very small and contain limited structural information.

B. 2D Prospectively Undersampling

Figure S15 and Table S1 give qualitative and quantitative results for 2D prospectively undersampled data reconstructed using patch-tensor LR, MLLR, GTLR, CG-SENSE, and patch-tensor L+S approaches with comparison to GRE fMRI. The patch-tensor LR, GTLR, and patch-tensor L+S models result in similar performances. The 2D prospectively undersampled data have better temporal resolution (by a factor of 9) than the 2D retrospectively undersampled data, which helps improve the quality of the data-shared initialization and thus the reconstructions.

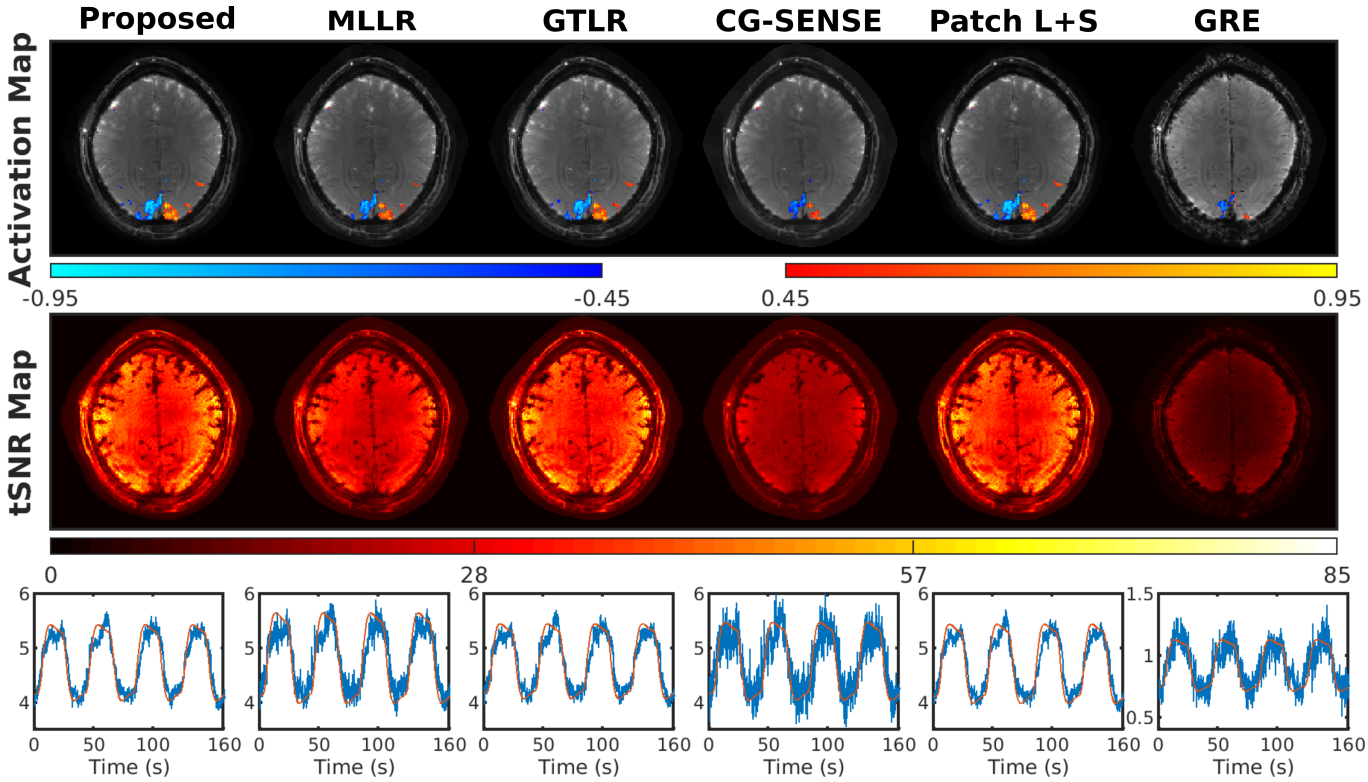

Fig. S15. Activation maps, temporal SNR maps, and time courses in the activated regions from prospectively undersampled reconstructions and GRE fMRI. A contiguity threshold of 2 was applied for the activation maps. The patch-tensor low-rank, global tensor low-rank, and patch-tensor low-rank plus sparse reconstructions outperform other approaches with more functional activation and cleaner time courses.

TABLE S1
QUANTITATIVE COMPARISONS OF OSSI 2D PROSPECTIVELY UNDERSAMPLED RECONSTRUCTIONS

	Proposed	MLLR	GTLR	CG-SENSE	Patch L+S	GRE
# Activated Voxels	322	233	311	149	324	83
Average tSNR	32.8	25.6	32.1	18.2	32.4	9.8

V. 4D Patch-Tensor and Multi-Scale Patch-Tensor Low-Rank Models

This section focuses on comparisons to other models including 4D patch-tensor low-rank and multi-scale patch-tensor low-rank. Instead of vectorizing the spatial dimensions as for the proposed 3D patch-tensor low-rank, 4D (or 5D for 3D OSSI fMRI with 2 time dimensions) patch-tensor low-rank model keeps all the spatial dimensions of the tensor for imposing low-rank constrains. The cost function is the same as equation (2) without vectorization of spatial dimensions in $\mathcal{P}_m$. The cost function for the multi-scale low-rank model we tested can be expressed as

$$\arg\min_{\mathbf{X}} \sum_{n=1}^{3} \sum_{m=1}^{M_n} \sum_{i=1}^{3} \lambda_i \left\| \mathcal{P}_m(\mathbf{X}_n)_{(i)} \right\|_* + \frac{1}{2} \left\| \mathcal{A}\left(\sum\nolimits_{n=1}^{3} \mathbf{X}_n \right) - \mathbf{y} \right\|_2^2, \tag{1}$$

where $\mathbf{X}_n$ is composed of scale-n patch-tensors. Specifically, we imposed tensor low-rank on patches of different spatial dimension 4×4, 8, and 14. Here, $\mathcal{P}(\cdot)$ partitions and reshapes the input into M_n low-rank patch-tensors for different scale n. The regularization parameters for the new models were also selected based on their impulse responses with similar magnitudes to the 3D patch-tensor LR model.

All three models are of similar reconstruction and functional performance. Figure S16 provides activation maps and tSNR maps of 3D patch-tensor LR, 4D patch-tensor LR, and multi-scale patch-tensor LR with comparison to the mostly sampled reconstruction. Quantitative evaluations including NRMSD and functional activation are in Table S2. Figure S17 shows the ROC curves for the models.

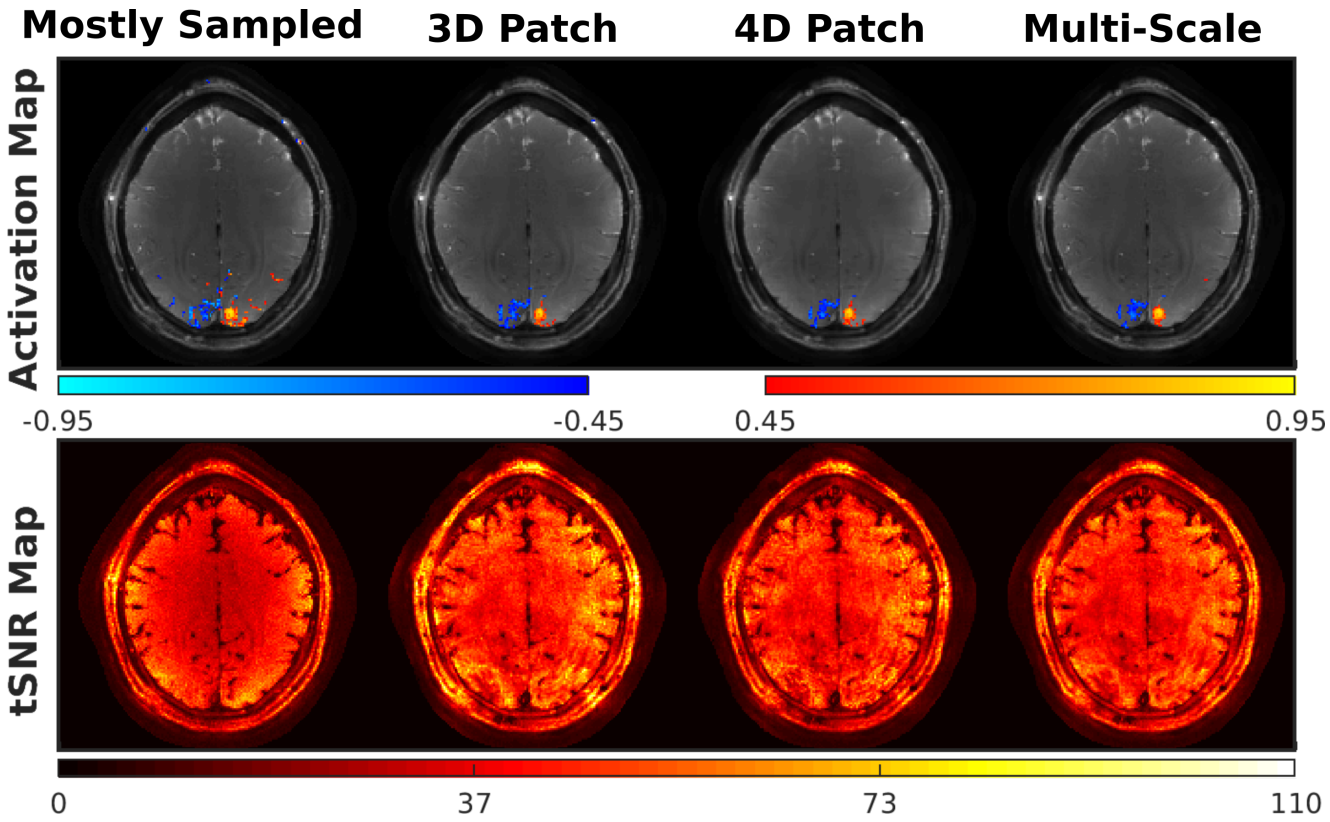

Fig. S16. Activation maps and temporal SNR maps from retrospectively undersampled data and reconstruction models including the proposed 3D patch-tensor low-rank, 4D patch-tensor low-rank, and multi-scale tensor low-rank. A contiguity threshold of 2 was applied for the activated regions. All three approaches perform well with similar amounts of activation and temporal SNR.

TABLE S2
QUANTITATIVE COMPARISONS OF OTHER OSSI 2D RETROSPECTIVELY UNDERSAMPLED RECONSTRUCTIONS

	Mostly Sampled	3D Patch	4D Patch	Multi-Scale
NRMSD Before Comb	-	0.17	0.19	0.17
NRMSD After Comb	-	0.05	0.06	0.05
# Activated Voxels	229	168	145	146
Average tSNR	37.1	43.6	41.4	41.2

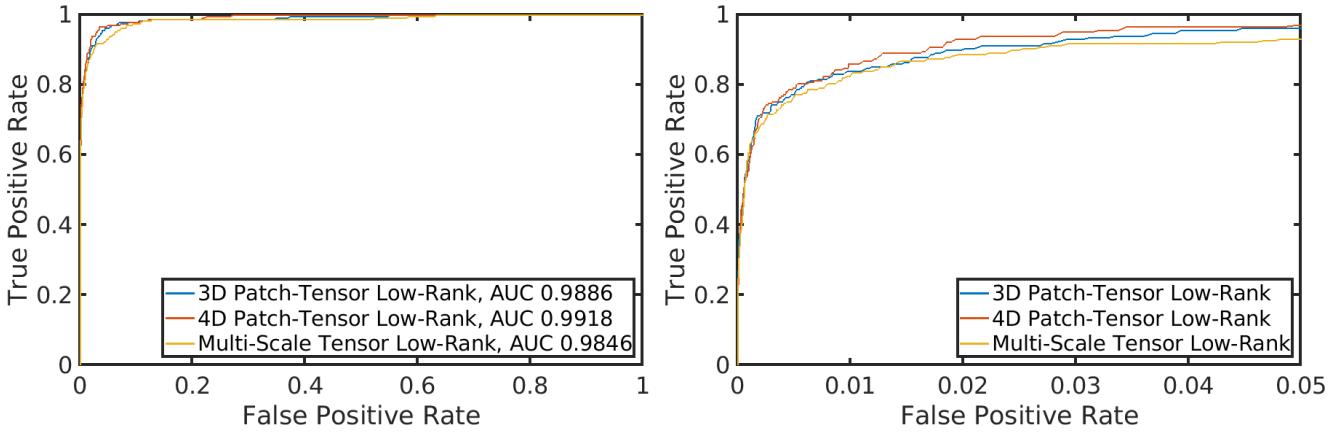

Fig. S17. ROC curves of different reconstruction models including the proposed 3D patch-tensor low-rank, 4D patch-tensor low-rank, and multi-scale tensor low-rank. The activation of the mostly sampled data at the lower third of the brain is used as ground truth. All three models perform well with large areas under the ROC curve (left), and the ROC curve of the 4D patch-tensor low-rank model is slightly closer to the top left corner than other approaches, especially for the reasonable range with false positive rate less than 0.05 (right).

VI. Other Subjects

This section presents 2D reconstruction results of a different subject. Both retrospectively and prospectively undersampled data were acquired with spiral-out trajectories. Retrospectively undersampled reconstruction results before and after 2-norm combination, and difference maps compared to the mostly sampled data are in Figure S18. Figure S19 presents functional activation maps and tSNR maps demonstrating that the proposed model outperforms other approaches with more activation. Table S3 summarises quantitative values of different reconstructions. Figure S20 provides ROC curves of the activation maps. 2D prospectively undersampled reconstruction results including activation maps, tSNR maps, and example time courses are given in Figure S21. Table S4 gives the corresponding quantitative evaluations.

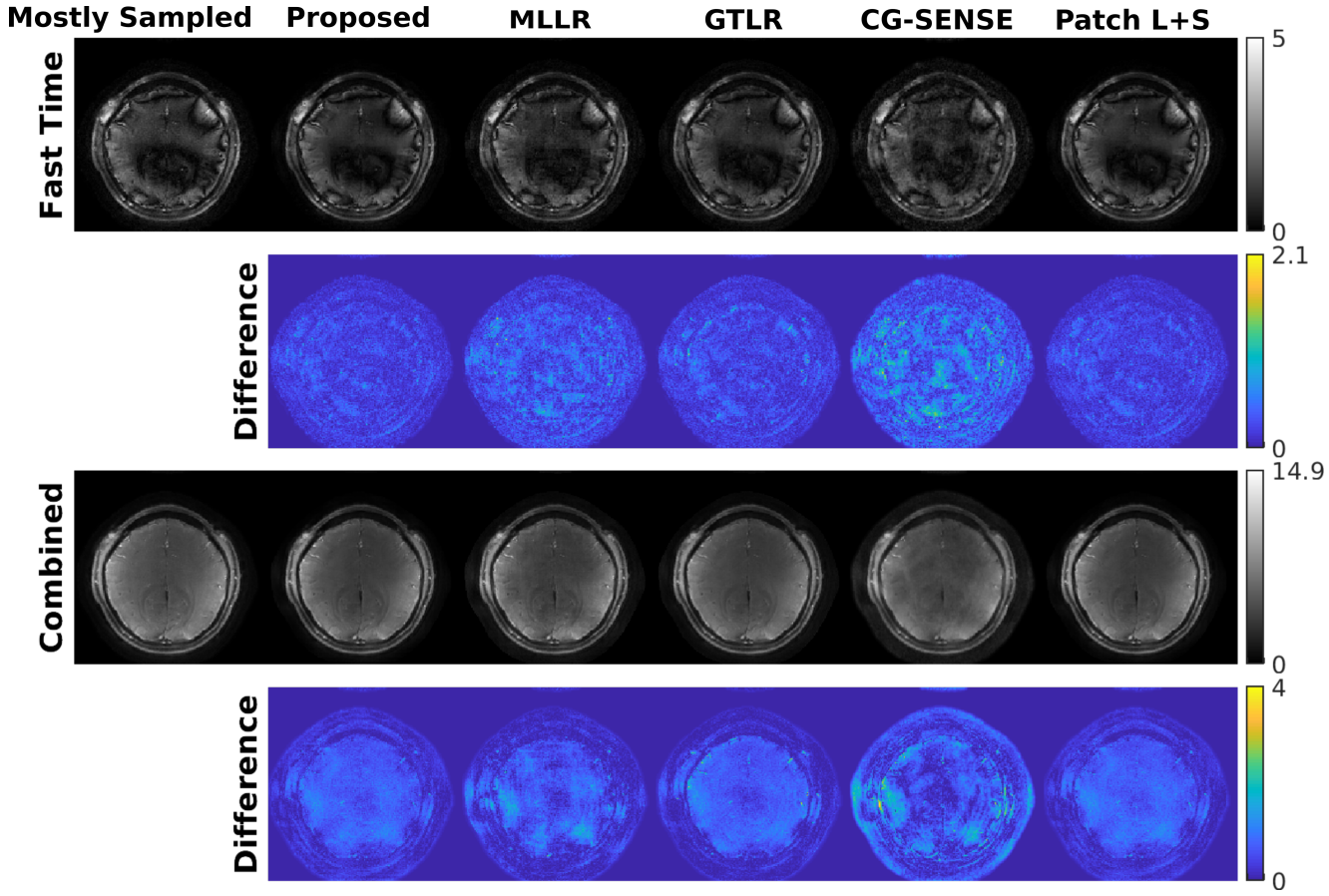

Fig. S18. The retrospectively undersampled reconstructions of a different subject are compared to the mostly sampled results. The proposed approach outperforms other methods with less noisy fast time images and less structure in the difference maps before and after combination.

TABLE S3
RETROSPECTIVELY UNDERSAMPLED RECONSTRUCTIONS OF A DIFFERENT SUBJECT

	Mostly Sampled	Proposed	MLLR	GTLR	CG-SENSE	Patch L+S
NRMSD Before Comb	-	0.19	0.28	0.2	0.36	0.2
NRMSD After Comb	-	0.12	0.13	0.13	0.14	0.13
# Activated Voxels	225	166	52	48	34	164
Average tSNR	40.2	41	25.2	46.1	19	42.1

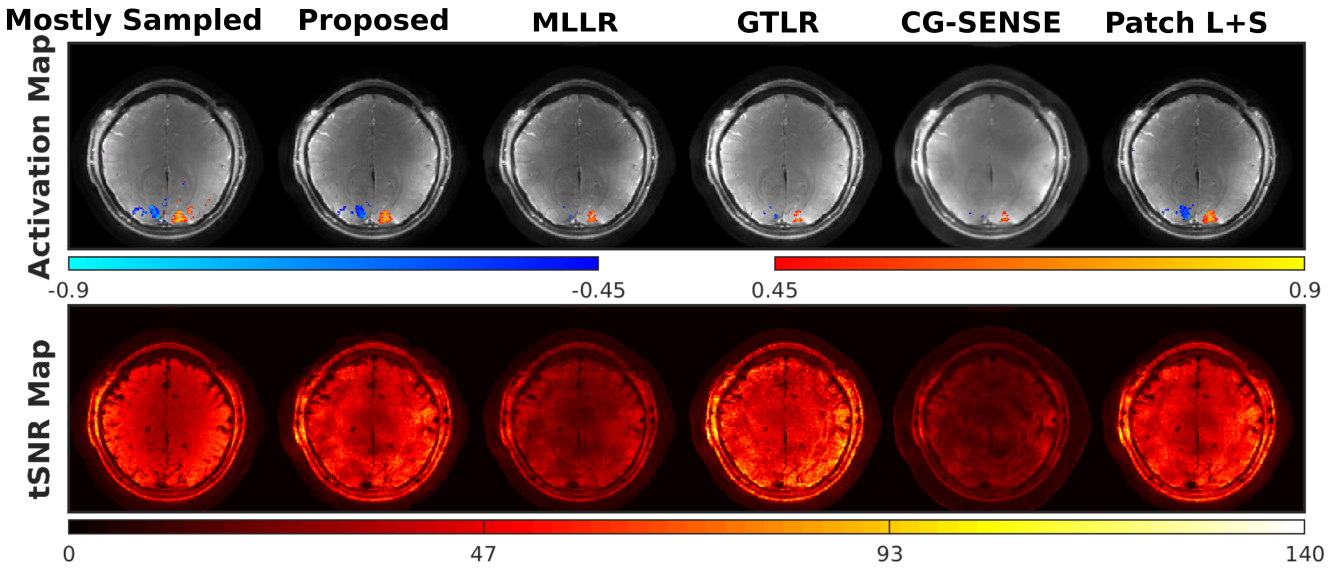

Fig. S19. Activation maps and temporal SNR maps from retrospectively undersampled reconstructions of a different subject. A contiguity (cluster-size) threshold of 2 was applied for the activated regions. The proposed model provides more functional activation than other approaches and shows similar results as the patch-tensor low-rank plus sparse model.

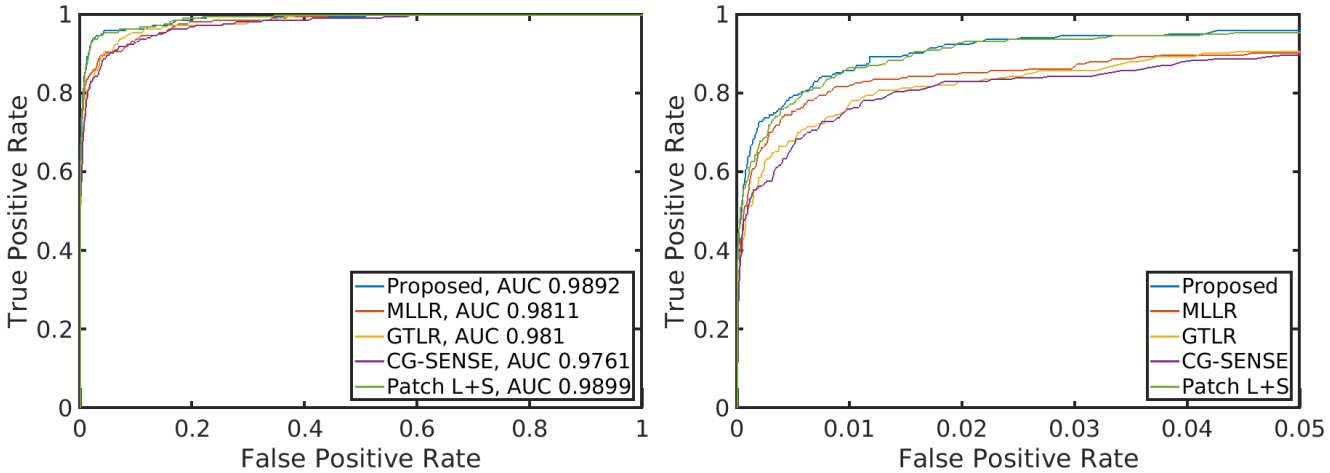

Fig. S20. ROC curves for a different subject with mostly sampled activation at the lower third of the brain as ground truth. The proposed method outperforms other approaches with the largest area under the ROC curve (left). The ROC curve of the proposed approach is also the closest to the top left corner, especially for the reasonable range with false positive rate less than 0.05 (right).

TABLE S4
PROSPECTIVELY UNDERSAMPLED RECONSTRUCTIONS OF A DIFFERENT SUBJECT

	Proposed	MLLR	GTLR	CG-SENSE	Patch L+S
# Activated Voxels	225	120	223	89	227
Average tSNR	33.5	21.1	34.9	20.6	34

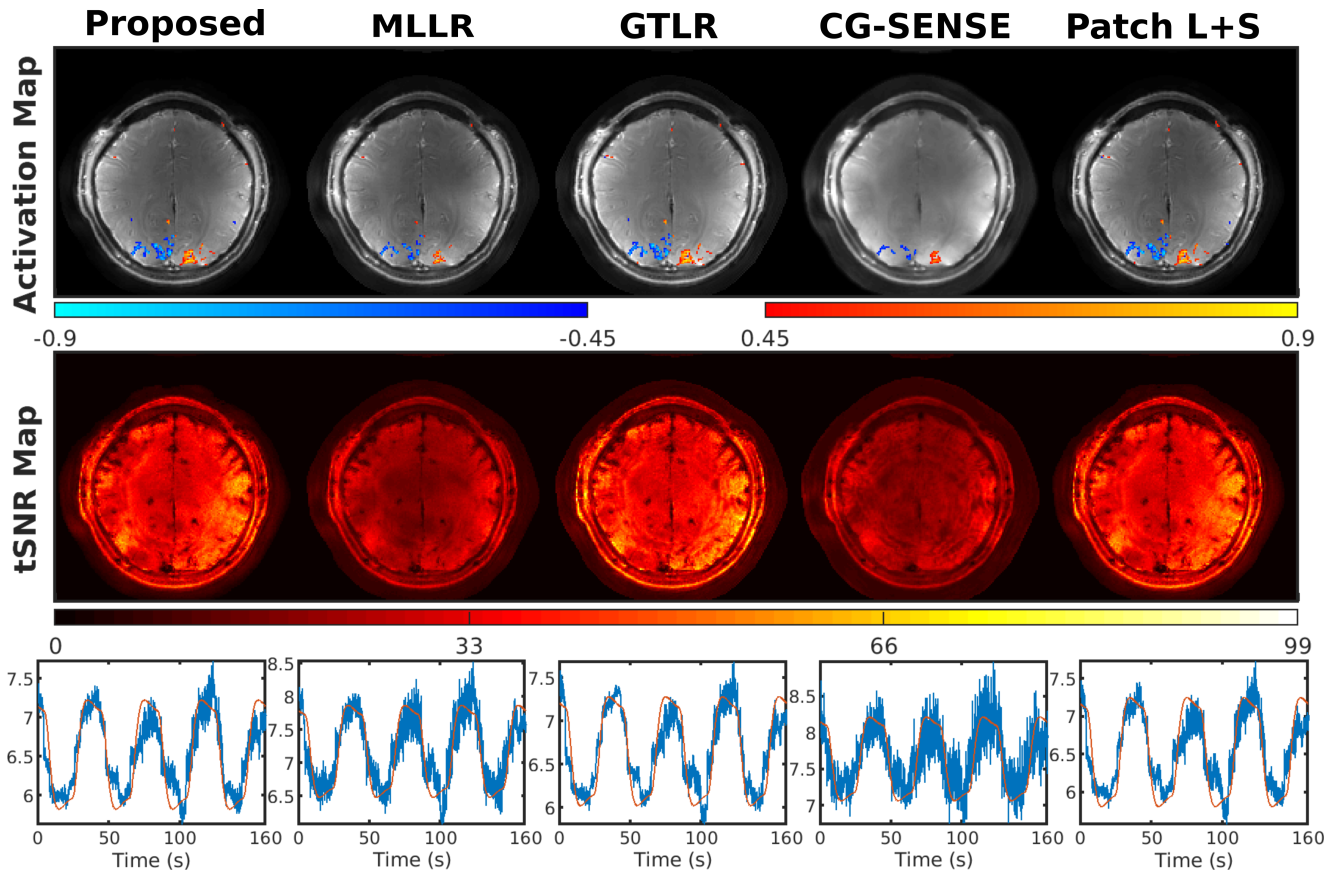

Fig. S21. Activation maps, temporal SNR maps, and activated time courses from prospectively undersampled reconstructions of a different subject. A contiguity (cluster-size) threshold of 2 was applied for the activation maps. The patch-tensor low-rank, global tensor low-rank, and patch-tensor low-rank plus sparse reconstructions outperform other approaches with more functional activation and cleaner time courses.